ARTICLE

Measurement-based quantum control of mechanical motion

Massimiliano Rossi[1,2,3], David Mason[1,2,3], Junxin Chen[1,2,3], Yeghishe Tsaturyan[1] & Albert Schliesser[1,2]*

Controlling a quantum system by using observations of its dynamics is complicated by the backaction of the measurement process—that is, the unavoidable quantum disturbance caused by coupling the system to a measurement apparatus. An efficient measurement is one that maximizes the amount of information gained per disturbance incurred. Real-time feedback can then be used to cancel the backaction of the measurement and to control the evolution of the quantum state. Such measurement–based quantum control has been demonstrated in the clean settings of cavity and circuit quantum electrodynamics, but its application to motional degrees of freedom has remained elusive. Here we demonstrate measurement–based quantum control of the motion of a millimetre–sized membrane resonator. An optomechanical transducer resolves the zero–point motion of the resonator in a fraction of its millisecond-scale coherence time, with an overall measurement efficiency close to unity. An electronic feedback loop converts this position record to a force that cools the resonator mode to its quantum ground state (residual thermal occupation of about 0.29). This occupation is nine decibels below the quantum–backaction limit of sideband cooling and six orders of magnitude below the equilibrium occupation of the thermal environment. We thus realize a long–standing goal in the field, adding position and momentum to the degrees of freedom that are amenable to measurement–based quantum control, with potential applications in quantum information processing and gravitational–wave detectors.

Controlling the state of a quantum system is a delicate task because any observation of the system will inevitably perturb it[1,2]. Coherent quantum control avoids this issue by coupling the system to another quantum system, a 'controller', in such a way that the joint system converges to the target state without the need for measurement, at the expense of quantum resources in the controller. Measurement-based quantum control[3–5] is based on a different paradigm. It exerts control by measuring the quantum state and applying feedback that depends on the measurement outcome, much like classical control systems. However, in the quantum regime, the effect of the backaction of the measurement must be taken into account, and effectively cancelled. This requires an overall measurement efficiency η—in essence, the amount of information gained per decoherence induced—close to unity. So far, this challenging demand has been met only in the clean settings of cavity and circuit quantum electrodynamics[6,7] (for example, $\eta = 40\%$ in ref. [7]).

To prepare high-purity motional quantum states, researchers have traditionally relied on sideband cooling, a form of coherent quantum control. An engineered quantum optical bath acts as the controller, to which the motional degree of freedom couples through optical forces. The motion thermalizes to this bath, at a temperature that is determined by the quantum fluctuations of the forces. This temperature sets a fundamental limit to sideband cooling. In optomechanics, this limit requires that the cavity linewidth resolves the motional sidebands to enable ground-state cooling with coherent light[8]. Systems that operate in this regime have been prepared close to the ground state[9,10], and cooling 2 dB below the sideband-cooling limit was demonstrated recently by squeezing the electromagnetic vacuum fluctuations[11].

Within the paradigm of measurement-based quantum control, feedback cooling[12,13] can overcome this limit, given a sufficiently efficient measurement. This protocol has been explored in several fields, including atomic physics, optomechanics and gravitational-wave astronomy. However, despite two decades of research involving diverse mechanical systems, such as trapped atoms[14], ions[15], micro- and nanoparticles[16,17], cantilevers[18,19], nanomechanical resonators[20–23], mirror modes[13] and gravitational-wave detector masses[24,25], ground-state cooling, an elementary form of quantum control, has yet to be achieved. This is chiefly because previous measurements were too weak ($\Gamma_{\mathrm{meas}} \ll \gamma$, where Γ_{meas} is the measurement rate[2] and γ is the motional decoherence rate due to coupling to the environment) and/or the detection too inefficient ($\Gamma_{\mathrm{meas}} \ll \Gamma_{\mathrm{qba}}$, where Γ_{qba} is the motional decoherence rate due to the quantum backaction of the measurement) to realize an overall measurement efficiency of $\eta = \Gamma_{\mathrm{meas}}/(\Gamma_{\mathrm{qba}} + \gamma) \approx 1$. The closest previous approach to this ideal-efficiency limit is reported in ref. [20], in which $\eta = 0.9\%$ was reached in a feedback experiment on a nanomechanical resonator.

In contrast to previous attempts, we perform a motion measurement that is sufficiently strong and efficient to reach $\eta = 56\%$. This high efficiency is enabled by an extremely precise displacement measurement, which realizes the closest approach so far (within 35%) to the Heisenberg measurement–disturbance uncertainty limit and the standard quantum limit.

Experimental setting

We study the drumhead-like motion of a highly tensioned, millimetre-sized, 20-nm-thick Si_3N_4 membrane (Fig. 1). The resonance mode of interest is confined to a defect within a phononic crystal, created by patterning a periodic array of holes into the membrane. The frequency of the defect mode $\Omega_{\mathrm{m}}/(2\pi) = 1.14$ MHz lies in the bandgap of the surrounding phononic crystal, which minimizes radiative leakage of mechanical energy into the surrounding structure. In addition, the gentle confinement by the phononic crystal reduces mode curvature compared to membranes clamped to a rigid substrate. As demonstrated recently[26], such soft clamping greatly suppresses mechanical energy dissipation (Γ_{m}) and enables ultrahigh quality factors $Q = \Omega_{\mathrm{m}}/\Gamma_{\mathrm{m}}$;

[1]Niels Bohr Institute, University of Copenhagen, Copenhagen, Denmark. [2]Center for Hybrid Quantum Networks (Hy-Q), Niels Bohr Institute, University of Copenhagen, Copenhagen, Denmark. [3]These authors contributed equally: Massimiliano Rossi, David Mason, Junxin Chen. *e-mail: albert.schliesser@nbi.ku.dk
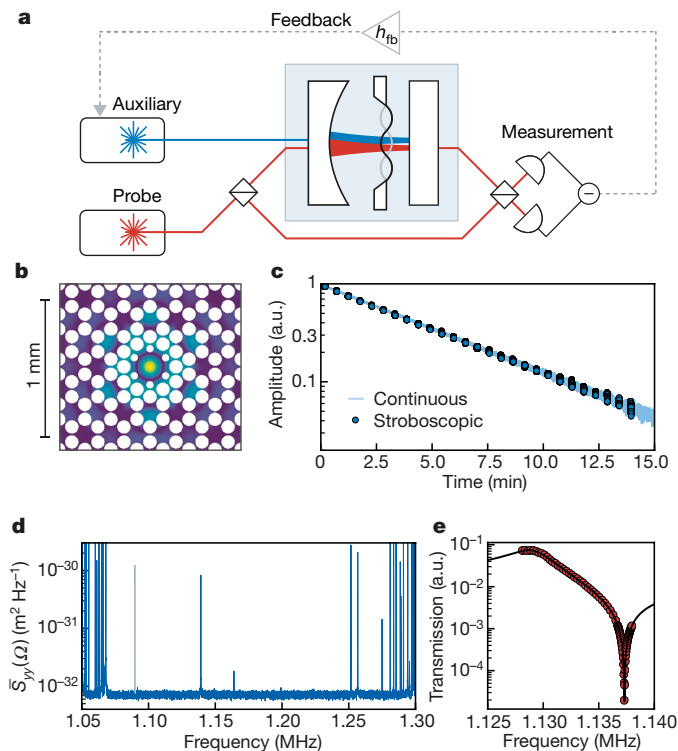
Fig. 1 | Optomechanical system. a, Sketch of experimental set-up. The mechanical resonator couples to a cryogenic optical cavity. Its motion is probed by a resonant laser (red), the phase of which is measured with a balanced homodyne detector. An additional auxiliary laser (blue) drives a different cavity mode. The probe signal can be used to control the auxiliary laser via an electronic feedback loop (h_{fb}). **b**, Simulated displacement pattern (colour scale; dark blue, small displacement; yellow, large displacement) of the mechanical mode of interest. The white circles correspond to holes in the membrane. **c**, Mechanical ringdown measurements. Light (dark) blue indicates continuously monitored (stroboscopic) ringdown. **d**, Displacement spectrum around the frequency region of the bandgap. Out-of-bandgap modes are visible at the edges of the spectrum, and five in-gap modes are visible. A phase calibration tone is shown in grey. **e**, An OMIT measurement (red symbols), used to characterize the optomechanical coupling strength (from the fit, black line). a.u., arbitrary units.

we find $Q = 1.03 \times 10^9$ in ringdown measurements, carefully ruling out artefacts (see Methods). This quality factor corresponds to a mechanical coherence time $\gamma^{-1} \approx (\bar{n}_{th}\Gamma_m)^{-1} = \hbar Q/(k_B T)$ (where $\hbar$ is the reduced Planck constant, k_B is the Boltzmann constant, T is the temperature of the environment and $\bar{n}_{th}$ is the occupation of the thermal bath) of the order of 1 ms, even at the moderate cryogenic temperatures ($T \approx 10$ K, $\bar{n}_{th} = \mathcal{O}(10^5)$) at which all reported experiments were conducted.

The membrane is introduced into a 1.6-mm-long, high-finesse Fabry–Pérot resonator, so that displacement by its zero-point amplitude $x_{zpf} = \sqrt{\hbar/(2m\Omega_m)}$ (where m is the mass of the resonator) dispersively shifts[27,28] (Methods) the optical-mode frequency by the vacuum optomechanical coupling rate g_0. Populating the cavity with a coherent field of average photon number $\bar{n}_{cav}$ then leads to the field-enhanced optomechanical coupling $g = g_0\sqrt{\bar{n}_{cav}}$ in a linearized, quantum-non-demolition-type interaction Hamiltonian $H' = -\hbar g(a^\dagger + a)(b^\dagger + b)$ between the shifted annihilation (creation) operators a ($a^\dagger$) and b ($b^\dagger$) of the cavity field and the mechanical motion, respectively[8,29]. A probe laser (Fig. 1a, red) is used to probe the frequency fluctuations of an optical cavity mode of linewidth $\kappa/(2\pi) = 15.9$ MHz. We measure the mechanical position by monitoring the phase of the transmitted light using balanced homodyne detection. In an unresolved sideband system ($\kappa \gg \Omega_m$), this measurement occurs at a rate[29] $\Gamma_{meas} = 4\eta_{det}g^2/\kappa$, for a detection efficiency η_{det}. Careful optimization of the entire detection chain (Methods) leaves us with $\eta_{det} = 77\%$.

In addition, we frequently use an auxiliary laser (Fig. 1a, blue), which populates a different longitudinal cavity mode (linewidth, $\kappa_{aux}/(2\pi) = 12.9$ MHz) and has a polarization that is orthogonal to the probe beam to avoid unwanted interference. This laser has several purposes, including laser cooling and, in combination with an amplitude modulator, exerting a force on the mechanical resonator via radiation pressure. Its exact role is specified in each section, in which the different experiments that we performed are described.

To gauge the possible strength of the measurement, we perform optomechanically induced transparency (OMIT) measurements[30] to extract g. We find (Fig. 1e) values up to $g/(2\pi) = 329$ kHz, which suggests that the effect of measurement-induced quantum backaction ($\Gamma_{qba} = 4g^2/\kappa$) exceeds that of thermal decoherence (γ) by a large margin. The ratio of these parameters defines the quantum cooperativity parameter[8,29] $C_q = \Gamma_{qba}/\gamma$; we achieve values of up to $C_q = 119$. We therefore expect a close-to-unity overall measurement efficiency $\eta = \eta_{det}/(1 + 1/C_q)$, as required for successful quantum control.
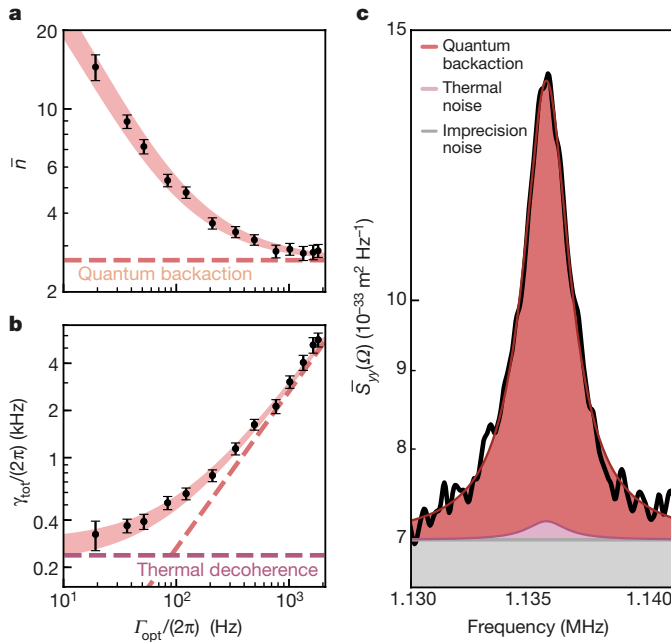
Quantum backaction in sideband cooling

For further characterization and direct comparison with a coherent control technique, we proceed with a sideband-cooling experiment. While monitoring the mechanical motion with a weak ($C_q \ll 1$), resonant probe beam, we lock the auxiliary laser (Fig. 1, with no feedback loop, $h_{fb} = 0$) at a finite detuning ($\Delta_{aux}/(2\pi) = -4.2$ MHz). Increasing the power of this auxiliary beam results in two competing processes: cooling of the motion by optical damping (at rate Γ_{opt}) and heating by quantum backaction (radiation-pressure quantum noise) on top of the constant thermal noise. At sufficiently high powers, these processes equilibrate[8,11,29,31] and the mechanical phonon occupancy $\bar{n} = (\Gamma_{opt}\bar{n}_{min} + \Gamma_m\bar{n}_{th})/(\Gamma_{opt} + \Gamma_m)$ asymptotes to the (sideband-cooling) quantum backaction limit $\bar{n}_{min} = [(\Omega_m + \Delta_{aux})^2 + (\kappa_{aux}/2)^2]/(-4\Delta_{aux}\Omega_m)$.

Comparison of this model with our data (Fig. 2) yields several conclusions. First, Fig. 2b confirms that the regime of dominating quantum backaction can indeed be accessed deeply ($\Gamma_{opt}\bar{n}_{min} \gg \Gamma_m\bar{n}_{th}$). Second, the quantum backaction limit ($\bar{n}_{min} = 2.64$) precludes sideband cooling to the ground state because of the 'bad' cavity ($\kappa_{aux} \approx \kappa \gg \Omega_m$) that we use. Third, the excellent agreement, even towards the highest Γ_{opt}, indicates the absence of substantial excess backaction, such as classical radiation-pressure noise. This finding is consistent with independent measurements of the noise of the lasers (Supplementary Information). Fourth, equilibration to an optical bath is beneficial for calibrating the vacuum optomechanical coupling rate g_0 of the probe using a standard frequency-modulation technique[32] (Methods), which requires reference data with known phonon occupation $\bar{n}$. The temperature of the phonon thermal bath $T \approx \bar{n}_{th}\hbar\Omega_m/k_B$ (which is usually difficult to ascertain) is negligible for the largest Γ_{opt}; it contributes only $(1 + \Gamma_{opt}\bar{n}_{min}/\Gamma_m\bar{n}_{th})^{-1} \approx 4\%$ to the occupation $\bar{n}$. Instead, $\bar{n} \approx \bar{n}_{min}$ is determined by only the parameters κ_{aux}, Δ_{aux} and Ω_m, which can be easily and robustly determined spectroscopically. In physical terms, this calibration means that we use vacuum fluctuations as a temperature reference[33] to extract g_0. A fit (Methods) to the whole dataset for all Γ_{opt}, based on standard theory of optomechanical sideband cooling[8], yields $g_0 = 2\pi \times (127 \pm 2)$ Hz and $T = 11 \pm 2$ K (where the uncertainties quoted indicate the confidence interval of the fit). This value of g_0 compares well to that of $g_0 = g/\sqrt{\bar{n}_{cav}} = 2\pi \times 129^{+2}_{-3}$ Hz (where the uncertainty indicates the full range of measured values) determined from an OMIT fit with a calibrated intracavity photon number $\bar{n}_{cav}$. Both methods are subject to different systematic uncertainties (Methods); their excellent agreement underscores a thorough understanding of our system and lends further support to the calibration of the measured spectra in terms of the number of quanta based on this value of g_0.

Quantum measurement

In the next experiment we characterize the quality of the measurement to gauge the possibility of overcoming the sideband-cooling limit via measurement-based quantum feedback with $\eta \approx 1$. We reduce the auxiliary laser power and arrange it to provide only mild pre-cooling

Fig. 2 | Quantum backaction in sideband cooling. a, b, Phonon number $\bar{n}$ (**a**) and total heating rate $\gamma_{\mathrm{tot}} = \bar{n}(\Gamma_{\mathrm{opt}} + \Gamma_{\mathrm{m}}) = \Gamma_{\mathrm{opt}}\bar{n}_{\mathrm{min}} + \Gamma_{\mathrm{m}}\bar{n}_{\mathrm{th}}$ (**b**) obtained from fitting calibrated displacement spectra (Γ_{m}, mechanical energy decay rate; Γ_{opt}, optical damping rate; $\bar{n}_{\mathrm{min}}$, occupancy in the sideband-cooling limit; $\bar{n}_{\mathrm{th}}$ occupancy of the thermal bath). The shaded areas show fits of a theoretical model to these data (Supplemetary Information), with the width reflecting the confidence interval of the fit. Dashed lines indicate contributions from thermal decoherence (purple) and quantum backaction (red). Error bars indicate two standard deviations. **c,** Calibrated displacement spectrum (black line) corresponding to the highest cooling power, with a Lorentzian fit (red line). The grey line represents the imprecision noise. Thermal noise (pink) contributes about 4% of the total force noise, the remainder being due to quantum backaction (red).

on the mechanical mode of interest ($\Gamma_{\mathrm{opt}}/(2\pi) = \mathcal{O}(10)$ Hz), and on all other modes of the membrane (Supplementary Information), to stabilize the system. At the same time, we increase the probe power in several steps into the regime $C_{\mathrm{q}} > 1$.

In Fig. 3 we show the corresponding measured mechanical displacement spectra $\bar{S}_{yy}(\Omega)$, obtained from the calibrated time-dependent homodyne photocurrent $y(t) = x(t) + x_{\mathrm{imp}}(t)$, which includes the actual mechanical position x and the measurement-imprecision noise x_{imp} (Supplementary Information). When increasing the probe strength, the imprecision noise floor decreases and the total force noise on the resonator increases due to quantum backaction. We fit the spectra to a Lorentzian peak, driven by a total force noise $\bar{S}_{FF}^{\mathrm{tot}}$ and with an imprecision noise floor $\bar{S}_{xx}^{\mathrm{imp}}$:

$$\bar{S}_{yy}(\Omega) = |\chi_{\mathrm{eff}}(\Omega)|^2\, \bar{S}_{FF}^{\mathrm{tot}} + \bar{S}_{xx}^{\mathrm{imp}} \qquad (1)$$

where $\chi_{\mathrm{eff}}(\Omega)$ is the effective mechanical susceptibility, with resonance frequency Ω_{eff} and damping Γ_{eff}, which is affected by the (largely irrelevant) dynamical backaction of the lasers[8,29].

For the sake of comparability, we reference these measurement noises to the resonant spectral density associated with mechanical zero-point fluctuations. Doing so yields the number of imprecision noise quanta $n_{\mathrm{imp}} = \bar{S}_{xx}^{\mathrm{imp}}/(8x_{\mathrm{zpf}}^2/\Gamma_{\mathrm{m}})$ and force noise quanta $n_{\mathrm{tot}} = \bar{S}_{FF}^{\mathrm{tot}}/(8p_{\mathrm{zpf}}^2/\Gamma_{\mathrm{m}})$, where p_{zpf} is the zero-point amplitude of the momentum such that $x_{\mathrm{zpf}}p_{\mathrm{zpf}} = \hbar/2$. For the strongest measurement we find $n_{\mathrm{imp}} = 5.8 \times 10^{-8}$. This constitutes an improvement of three orders of magnitude over the best previous measurement[20]. All measured values agree with the expectation $n_{\mathrm{imp}} = \Gamma_{\mathrm{m}}/(16\Gamma_{\mathrm{meas}})$ to within a factor of 1.03 ± 0.06 (where the uncertainties correspond to ± 1 standard deviation). The force acting on the system can be broken down into three contributions,

$\bar{S}_{FF}^{\mathrm{tot}} = \bar{S}_{FF}^{\mathrm{th}} + \bar{S}_{FF}^{\mathrm{aux}} + \bar{S}_{FF}^{\mathrm{qba}}$, due to thermal noise and quantum backaction of the auxiliary and probe beams. For each dataset, the fit results agree with the $\bar{S}_{FF}^{\mathrm{tot}}$ predicted from the parameters of the system (Supplementary Information) to within a factor of 1.08 ± 0.02 (where the uncertainties correspond to ± 1 standard deviation), with $\bar{S}_{FF}^{\mathrm{aux}}/\bar{S}_{FF}^{\mathrm{th}} \approx 0.18$ and $\bar{S}_{FF}^{\mathrm{qba}}/\bar{S}_{FF}^{\mathrm{th}} = C_{\mathrm{q}}$.

We use these findings to evaluate the measurement efficiency of the probe, $\eta = (16n_{\mathrm{imp}}n_{\mathrm{tot}})^{-1} = 56\%$, which is on par with circuit quantum electrodynamics systems[7] and sufficient to exert high-fidelity quantum control. Using $\eta = \hbar^2/(\bar{S}_{xx}^{\mathrm{imp}}\bar{S}_{FF}^{\mathrm{tot}})$ further allows comparison to the Heisenberg measurement–disturbance uncertainty relation[1,8,29] $\sqrt{\bar{S}_{xx}^{\mathrm{imp}}\bar{S}_{FF}^{\mathrm{qba}}} \geq \hbar$. The measured total noises $1.33\hbar = \sqrt{\bar{S}_{xx}^{\mathrm{imp}}\bar{S}_{FF}^{\mathrm{tot}}} \geq \sqrt{\bar{S}_{xx}^{\mathrm{imp}}\bar{S}_{FF}^{\mathrm{qba}}}$ constrain the deviation from an ideal measurement to at most 33%. To our knowledge, this is the best mechanical realization of the Heisenberg microscope gedanken-experiment so far. Consequently, the experimental displacement sensitivity of equation (1) is also closer to the standard quantum limit (SQL) than that of any previous measurement of this kind. We find that away from the mechanical resonance ($\delta\Omega = \Omega - \Omega_{\mathrm{eff}} \approx 2\pi \times 3.3$ kHz), at which the uncorrelated imprecision and backaction noises are optimally balanced, our mechanical sensor reaches $\bar{S}_{yy}(\Omega_{\mathrm{eff}} + \delta\Omega) = 1.35\bar{S}_{yy}^{\mathrm{SQL}}(\Omega_{\mathrm{eff}} + \delta\Omega)$, where $\bar{S}_{yy}^{\mathrm{SQL}}(\Omega) = 2\hbar\,|\chi_{\mathrm{eff}}(\Omega)|$. This result is better than what is currently achievable in Advanced LIGO[34], with ultracold atoms[35] or with ultracold mechanical resonators[10], even when probed with squeezed light[11] or with nominally sub-SQL variational techniques[36].

Ground-state cooling by feedback

We now use the signal $y(t)$ obtained from this near-ideal quantum measurement to control and stabilize the quantum state of the mechanical system. We electronically convolve the signal with a filter kernel $h_{\mathrm{fb}}(t)$ and apply the output $F_{\mathrm{fb}}(t) = h_{\mathrm{fb}}(t) * y(t)$ as a force to the mechanical resonator (feedback interaction, $H_{\mathrm{fb}} = F_{\mathrm{fb}}(t)x(t)$). To exert this force we modulate the amplitude of the auxiliary laser beam, the power of which is kept small, as in the previous experiment. In the domain of linearized quantum optomechanics, assuming Gaussian noise only, the quantum dynamics of the system can be mapped to a classical control problem, with the caveat that process and measurement noises must be included that mimic the quantum-mechanically required backaction and imprecision, respectively. Linear–quadratic–Gaussian control theory then provides a straightforward way of obtaining the optimum controller for cooling, the objective of which is to reduce a quadratic cost function—in this case, the mechanical position and momentum variance of a single mechanical mode[3,4,29,37–39] (Supplementary Information).

Although inspired by these results, our feedback filter $h_{\mathrm{fb}}(\Omega) = h_{\mathrm{main}}(\Omega) + h_{\mathrm{aux}}(\Omega)$, with

$$h_{\mathrm{main}}(\Omega) = g_{\mathrm{fb}}e^{i\Omega\tau - i\phi}\left(\frac{\Gamma_{\mathrm{fb}}\Omega}{\Omega_{\mathrm{fb}}^2 - \Omega^2 - i\Gamma_{\mathrm{fb}}\Omega}\right)^2 \qquad (2)$$

accommodates a more complex experimental reality (Supplementary Information). In particular, it contains a predominantly electronic loop delay of $\tau \approx 300$ ns, a high-order bandpass filter (with bandwidth Γ_{fb}, gain g_{fb} and global phase ϕ) peaked at the centre frequency Ω_{fb}, close to the centre of the phononic bandgap, to suppress gain for out-of-gap modes, and an auxiliary filter h_{aux} that suppresses instabilities of other mechanical modes far away from Ω_{m}. The phase ϕ is electronically adjusted so that $\arg(h_{\mathrm{fb}}(\Omega_{\mathrm{m}})) \approx -\pi/2$. The feedback force is then approximately proportional to the velocity of the resonator, providing a quantum-noise-limited friction force, which is sometimes referred to as 'cold damping'[12,13,40]. Together with standard optomechanical theory[8,29], equation (2) can be incorporated into a simple control-theoretical model that predicts the spectra of the measured displacement, $\bar{S}_{yy}(\Omega)$, and the underlying fluctuations in the position and momentum of the resonator, $\bar{S}_{xx}(\Omega)$ and $\bar{S}_{pp}(\Omega)$, respectively (Supplementary Information).
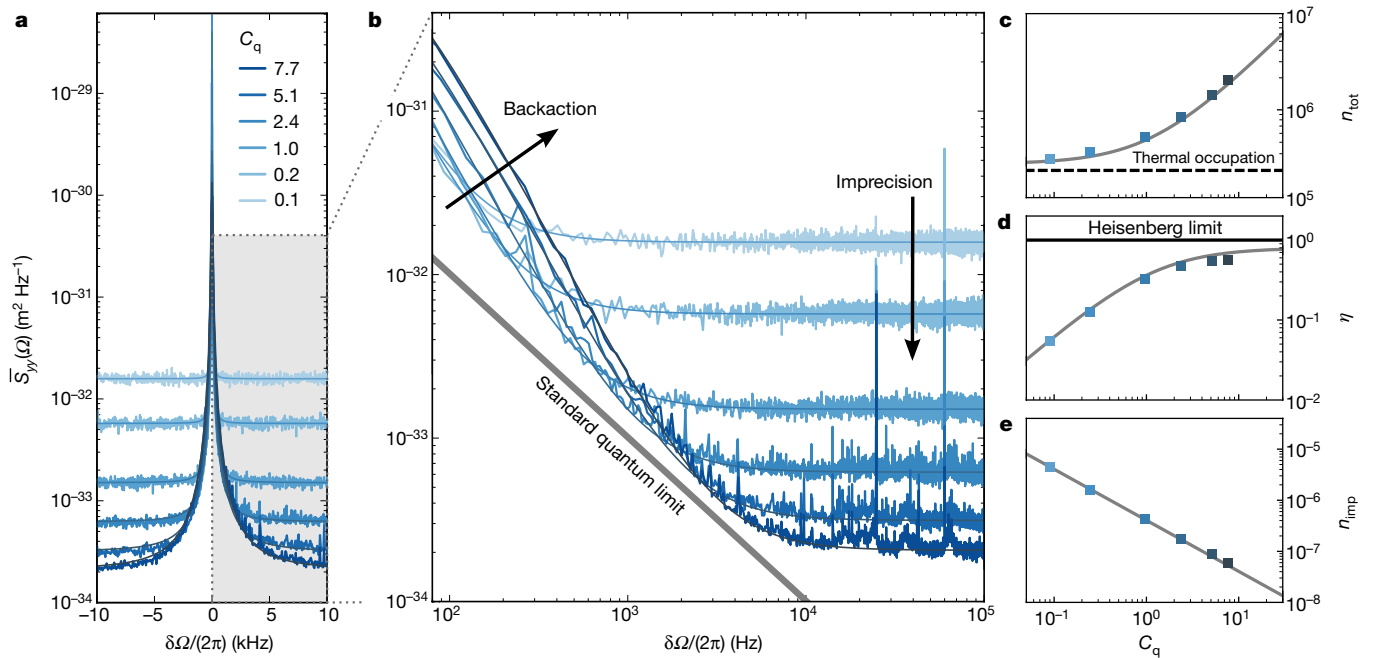
Fig. 3 | Quantum measurement. a, Displacement spectra around the effective mechanical frequency Ω_{eff}, for different quantum cooperativities C_q of the probe. **b**, Off-resonant tails of the spectra from **a** with Lorentzian fits (smooth, slightly darker lines). The standard quantum limit is indicated by the grey line. **c**, **e**, Imprecision noise n_{imp} (**e**) and the total force noise n_{tot} (**c**), from the fits in **b**. The former is visible as a decrease in the noise floor, whereas the latter appears as an increase in the wings of the Lorentzian (see arrows in **b**). The black dashed line in **c** indicates the thermal occupation. **d**, From these values, we calculate the measurement efficiency $\eta = 1/(16 n_{\mathrm{imp}} n_{\mathrm{tot}})$, which reaches 0.56. The Heisenberg limit corresponds to ideal efficiency, $\eta = 1$. The grey lines in **c**–**e** are fits of a theoretical model to the data (Supplementary Information).

To assess the cooling performance, we fit the predicted $\bar{S}_{yy}(\Omega)$ to measured spectra, adjusting n_{tot}, n_{imp}, g_{fb} and ϕ. The fit values for n_{tot} and n_{imp} agree with independent, first-principles calculations to within factors of 1.06 ± 0.07 and 1.01 ± 0.05, respectively (where the uncertainties correspond to ± 1 standard deviation). We then calculate the occupation of the mechanical resonator from its position variance:

$$\bar{n} = \langle b^\dagger b \rangle \approx \frac{1}{2}\left(\frac{1}{2\pi} \int_0^\infty \bar{S}_{xx}(\Omega) x_{\mathrm{zpf}}^{-2} \mathrm{d}\Omega - 1 \right)$$

In Fig. 4 we show the results as a function of controller gain (expressed as the effective resonator damping $\Gamma_{\mathrm{eff}} = \Gamma_{\mathrm{m}} + \mathrm{Im}[h_{\mathrm{fb}}(\Omega_{\mathrm{m}})]/(m\Omega_{\mathrm{m}}) + \Gamma_{\mathrm{opt}}$), for five different probing strengths up to $C_q = 7.8$. For each C_q, a minimum occupancy is reached for a certain gain, beyond which the resonator is heated again. This mechanism is known as noise 'squashing'[13,18,20] (Fig. 4b) and involves substantial imprecision noise being fed back to the mechanics. The lowest residual occupation observed is $\bar{n} = 0.29 \pm 0.03$ (where the uncertainty indicates the confidence interval of the fit; Fig. 4a).

We benchmark this cooling performance against the occupation $\bar{n}_{\mathrm{est}}$ of the conditional state (that is, conditioned on the measurement
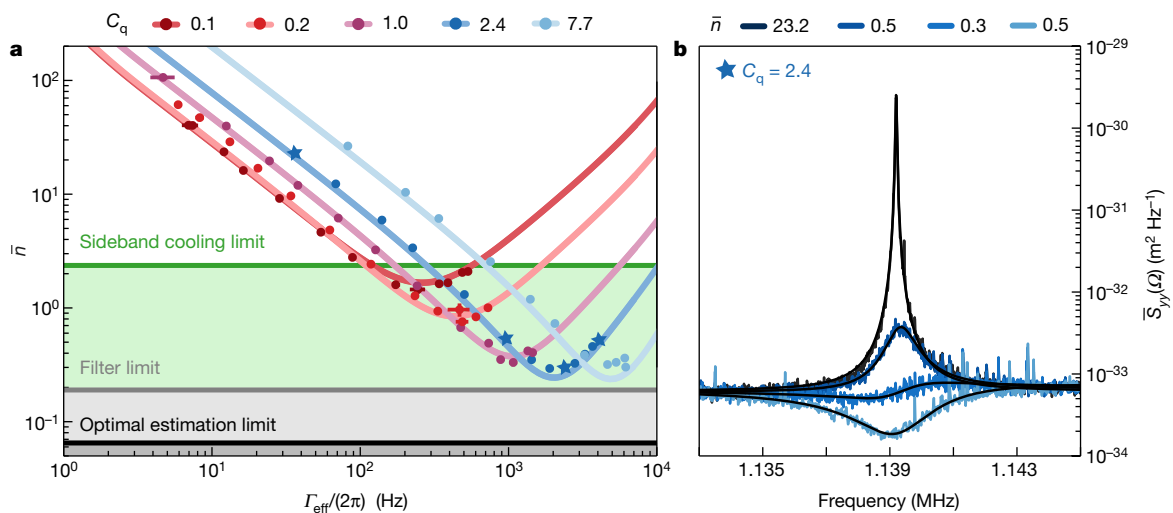
Fig. 4 | Feedback cooling to the quantum ground state. a, Mechanical occupancy for different quantum cooperativities C_q, as a function of loop gain, expressed here as an effective damping rate Γ_{eff}. Points are data; error bars indicate fit uncertainty; solid lines are theoretical calculations using independently estimated system parameters. The sideband-cooling limit for this system is shown as a green line. Grey and black lines indicate the limit of our implemented filter and of optimal state estimation, respectively (Supplementary Information). **b**, Exemplary spectra for $C_q = 2.4$, at the gain values marked by stars in **a**. Smooth black lines are Lorentzian fits.
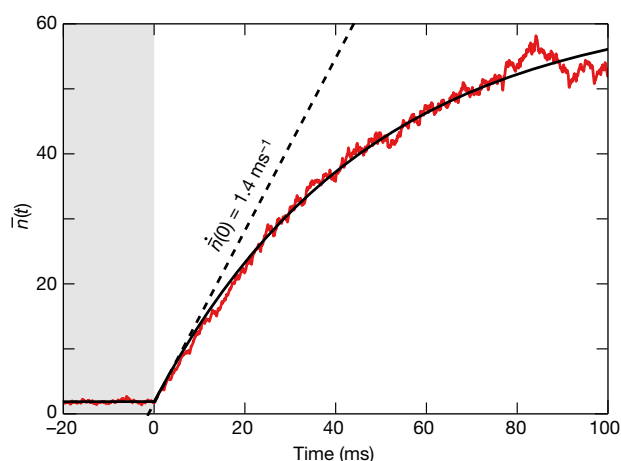
Fig. 5 | Heating from low phonon occupancy. Mechanical heating $\bar{n}(t)$ (red trace) measured by switching off the feedback at $t = 0$ ms. The black line is an exponential fit; its dashed tangent indicates $\dot{\bar{n}}(t = 0) \approx \gamma_{\mathrm{tot}}$. The grey shading indicates the time interval during which the feedback is applied.

result)[29,41,42]. The lowest conditional occupation is reached by optimal state estimation from the available measurement record and coincides with the lowest occupation to which ideal feedback can bring the resonator. Under the idealized assumption of a single-mode, high-Q resonator coupled to a hot thermal bath[29,41], $\bar{n}_{\mathrm{est}} \approx (\sqrt{1/\eta} - 1)/2$. This expression yields $\bar{n}_{\mathrm{est}} \approx 0.07$ for our $\eta_{\mathrm{det}} = 0.77$ and for $C_q \to \infty$, which corresponds to a state of high purity ($(1 + 2\bar{n}_{\mathrm{est}})^{-1} \approx 88\%$). The discrepancy with the achieved occupation indicates further room for improvement in engineering our feedback filter, the sub-optimal nature of which becomes apparent for high quantum cooperativity and gain (Supplementary Information). The performance compromise is a consequence of the need to avoid instabilities anywhere outside the bandgap—spectral regions that are crowded with other high-quality mechanical modes. Wider bandgaps, reduced loop delay and a filter that accounts for individual out-of-band modes are therefore routes to improved feedback.

By turning off the electronic feedback abruptly after cooling close to the ground state, we measure the heating rate of the resonator directly. In Fig. 5 we show the result of such a measurement, averaged over about 400 experimental iterations. The occupancy $\bar{n}(t)$ equilibrates exponentially to the level given by residual sideband cooling. At low probe power, we infer (Supplementary Information) a heating rate of 1.4 phonons per millisecond out of the ground state from the slope of this curve at $t = 0$ ms. This rate is consistent with the expected thermal decoherence rate $\gamma \approx \bar{n}_{\mathrm{th}} \Gamma_{\mathrm{m}}$ at the temperature of this experiment ($T \approx 9$ K) plus a contribution of 0.2 phonons per millisecond due to quantum backaction.

Discussion and outlook

Such millisecond coherence times compare favourably with other mechanical systems held at dilution refrigerator temperatures[11,31,43] and might be boosted to seconds if our system were made similarly cold. The very narrow linewidth of the mechanical mode (about 1 mHz) furthermore suggests the absence of substantial dephasing (Methods). Quantum memory applications are therefore conceivable.

With an overall measurement efficiency close to unity, mechanical systems such as the one presented here will allow tests and application of a wide range of quantum measurement and control techniques[3,4,29]. This includes time-continuous Bell measurements for state teleportation and entanglement swapping[44,45] and combination with mechanical parametric amplification[46] to create strongly squeezed mechanical states. An occupancy 9 dB below the sideband-cooling limit is promising for quantum control, in particular, of low-frequency mechanical systems such as those used for gravitational-wave detection;

feedback-based protocols to enhance interferometric detectors have already been proposed[47]. Combination with nonlinear measurement schemes, such as photon counting[48], could allow non-Gaussian state preparation. Moreover, given that we achieved $C_q > 100$ at 10 K, the prospect of quantum control of motion at room temperature appears more realistic than ever.

Online content

1. Braginsky, V. B. & Khalili, F. Y. *Quantum Measurement* (Cambridge Univ. Press, Cambridge, 1992).
2. Clerk, A. A., Devoret, M. H., Girvin, S. M., Marquardt, F. & Schoelkopf, R. J. Introduction to quantum noise, measurement, and amplification. *Rev. Mod. Phys.* **82**, 1155–1208 (2010).
3. Jacobs, K. *Quantum Measurement Theory and its Application* (Cambridge Univ. Press, Cambridge, 2014).
4. Wiseman, H. M. & Milburn, G. J. *Quantum Measurement and Control* (Cambridge Univ. Press, Cambridge, 2009).
5. Zhang, J., Liu, Y.-X., Wu, R.-B., Jacobs, K. & Nori, F. Quantum feedback: theory, experiments, and applications. *Phys. Rep.* **679**, 1–60 (2017).
6. Sayrin, C. et al. Real-time quantum feedback prepares and stabilizes photon number states. *Nature* **477**, 73–77 (2011).
7. Vijay, R. et al. Stabilizing Rabi oscillations in a superconducting qubit using quantum feedback. *Nature* **490**, 77–80 (2012).
8. Aspelmeyer, M., Kippenberg, T. J. & Marquardt, F. Cavity optomechanics. *Rev. Mod. Phys.* **86**, 1391–1452 (2014).
9. Chan, J. et al. Laser cooling of a nanomechanical oscillator into its quantum ground state. *Nature* **478**, 89–92 (2011).
10. Teufel, J. D. et al. Sideband cooling of micromechanical motion to the quantum ground state. *Nature* **475**, 359–363 (2011).
11. Clark, J. B., Lecocq, F., Simmonds, R. W., Aumentado, J. & Teufel, J. D. Sideband cooling beyond the quantum backaction limit with squeezed light. *Nature* **541**, 191–195 (2017).
12. Mancini, S., Vitali, D. & Tombesi, P. Optomechanical cooling of a macroscopic oscillator by homodyne feedback. *Phys. Rev. Lett.* **80**, 688–691 (1998).
13. Cohadon, P. F., Heidmann, A. & Pinard, M. Cooling of a mirror by radiation pressure. *Phys. Rev. Lett.* **83**, 3174–3177 (1999).
14. Kubanek, A. et al. Photon-by-photon feedback control of a single-atom trajectory. *Nature* **462**, 898–901 (2009).
15. Bushev, P. et al. Feedback cooling of a single trapped ion. *Phys. Rev. Lett.* **96**, 043003 (2006).
16. Li, T., Kheifets, S. & Raizen, M. G. Millikelvin cooling of an optically trapped microsphere in vacuum. *Nat. Phys.* **7**, 527–530 (2011).
17. Jain, V. et al. Direct measurement of photon recoil from a levitated nanoparticle. *Phys. Rev. Lett.* **116**, 243601 (2016).
18. Poggio, M., Degen, C. L., Mamin, H. J. & Rugar, D. Feedback cooling of a cantilever's fundamental mode below 5 mK. *Phys. Rev. Lett.* **99**, 017201 (2007).
19. Kleckner, D. & Bouwmeester, D. Sub-kelvin optical cooling of a micromechanical resonator. *Nature* **444**, 75–78 (2006).
20. Wilson, D. J. et al. Measurement-based control of a mechanical oscillator at its thermal decoherence rate. *Nature* **524**, 325–329 (2015).
21. Lee, K. H., McRae, T. G., Harris, G. I., Knittel, J. & Bowen, W. P. Cooling and control of a cavity optoelectromechanical system. *Phys. Rev. Lett.* **104**, 123604 (2010).
22. LaHaye, M. D., Buu, O., Camarota, B. & Schwab, K. C. Approaching the quantum limit of a nanomechanical resonator. *Science* **304**, 74–77 (2004).
23. Gavartin, E., Verlot, P. & Kippenberg, T. J. A hybrid on-chip optomechanical transducer for ultrasensitive force measurements. *Nat. Nanotechnol.* **7**, 509–514 (2012).
24. Vinante, A. et al. Feedback cooling of the normal modes of a massive electromechanical system to submillikelvin temperature. *Phys. Rev. Lett.* **101**, 033601 (2008).
25. Abbott, B. et al. Observation of a kilogram-scale oscillator near its quantum ground state. *New J. Phys.* **11**, 073032 (2009).
26. Tsaturyan, Y., Barg, A., Polzik, E. S. & Schliesser, A. Ultracoherent nanomechanical resonators via soft clamping and dissipation dilution. *Nat. Nanotechnol.* **12**, 776–783 (2017).
27. Thompson, J. et al. Strong dispersive coupling of a high-finesse cavity to a micromechanical membrane. *Nature* **452**, 72–75 (2008).
28. Nielsen, W. H. P., Tsaturyan, Y., Møller, C. B., Polzik, E. S. & Schliesser, A. Multimode optomechanical system in the quantum regime. *Proc. Natl Acad. Sci. USA* **114**, 62–66 (2017).
29. Bowen, W. P. & Milburn, G. J. *Quantum Optomechanics* 103, 161, 163 (CRC Press, Boca Raton, 2016).
30. Weis, S. et al. Optomechanically induced transparency. *Science* **330**, 1520–1523 (2010).
31. Peterson, R. W. et al. Laser cooling of a micromechanical membrane to the quantum backaction limit. *Phys. Rev. Lett.* **116**, 063601 (2016).

32. Gorodetksy, M., Schliesser, A., Anetsberger, G., Deleglise, S. & Kippenberg, T. Determination of the vacuum optomechanical coupling rate using frequency noise calibration. *Opt. Express* **18**, 23236–23246 (2010).
33. Purdy, T. P., Grutter, K. E., Srinivasan, K. & Taylor, J. M. Quantum correlations from a room-temperature optomechanical cavity. *Science* **356**, 1265–1268 (2017).
34. Martynov, D. V. et al. Sensitivity of the advanced LIGO detectors at the beginning of gravitational wave astronomy. *Phys. Rev. D* **93**, 112004 (2016).
35. Schreppler, S. et al. Optically measuring force near the standard quantum limit. *Science* **344**, 1486–1489 (2014).
36. Kampel, N. S. et al. Improving broadband displacement detection with quantum correlations. *Phys. Rev. X* **7**, 021008 (2017).
37. Doherty, A. C. & Jacobs, K. Feedback control of quantum systems using continuous state estimation. *Phys. Rev. A* **60**, 2700–2711 (1999).
38. Doherty, A. C., Habib, S., Jacobs, K., Mabuchi, H. & Tan, S. M. Quantum feedback control and classical control theory. *Phys. Rev. A* **62**, 012105 (2000).
39. Garbini, J. L., Bruland, K. J., Dougherty, W. M. & Sidles, J. A. Optimal control of force microscope cantilevers. l. Controller design. *J. Appl. Phys*. **80**, 1951–1958 (1996).
40. Genes, C., Vitali, D., Tombesi, P., Gigan, S. & Aspelmeyer, M. Ground-state cooling of a micromechanical oscillator: comparing cold damping and cavity-assisted cooling schemes. *Phys. Rev. A* **77**, 033804 (2008).
41. Doherty, A. C., Szorkovszky, A., Harris, G. I. & Bowen, W. P. The quantum trajectory approach to quantum feedback control of an oscillator revisited. *Phil. Trans. R. Soc. Lond. A* **370**, 5338–5353 (2012).
42. Wieczorek, W. et al. Optimal state estimation for cavity optomechanical systems. *Phys. Rev. Lett.* **114**, 223601 (2015).
43. Chu, Y. et al. Quantum acoustics with superconducting qubits. *Science* **358**, 199–202 (2017).
44. Hofer, S. G., Vasilyev, D. V., Aspelmeyer, M. & Hammerer, K. Time-continuous Bell measurements. *Phys. Rev. Lett.* **111**, 170404 (2013).
45. Hofer, S. G. & Hammerer, K. Entanglement-enhanced time-continuous quantum control in optomechanics. *Phys. Rev. A* **91**, 033822 (2015).
46. Szorkovszky, A., Doherty, A. C., Harris, G. I. & Bowen, W. P. Mechanical squeezing via parametric amplification and weak measurement. *Phys. Rev. Lett.* **107**, 213603 (2011).
47. Courty, J.-M., Heidmann, A. & Pinard, M. Quantum locking of mirrors in interferometers. *Phys. Rev. Lett.* **90**, 083601 (2003).
48. Ringbauer, M., Weinhold, T. J., Howard, L. A., White, A. G. & Vanner, M. R. Generation of mechanical interference fringes by multi-photon counting. *New J. Phys*. **20**, 053042 (2018).

METHODS

Soft-clamped mechanical resonator. The mechanical device used in the experiment is based on a 20 nm × 3.6 mm × 3.6 mm soft-clamped Si$_3$N$_4$ membrane[26]. As shown in Extended Data Fig. 1, a honeycomb hole pattern is fabricated into the membrane, producing phononic bandgaps for out-of-plane modes. In the centre of the membrane, a defect is created, supporting localized vibrational modes whose frequencies lie in one of these bandgaps. These mechanical modes are soft-clamped in the sense that their mode shapes decay into the phononic crystal structure gradually, as opposed to being clamped by a rigid frame. This reduced curvature, combined with stress redistribution due to the phononic pattern, results in ultrahigh mechanical quality factors. Here we focus on mode A, at $\Omega_m/(2\pi) = 1.139$ MHz. Compared to previous work[26], a modified defect design is used to shift mode A away from the left bandgap edge.

To measure the quality factor of this soft-clamped mode, we performed ringdown experiments. The laser is tuned to a wavelength where the finesse of the optical cavity is low ($F = \mathcal{O}(10)$), allowing interferometric displacement measurements without dynamical optomechanical effects. The transmitted light intensity is measured directly with a photodiode, and the photocurrent is demodulated at the mechanical frequency Ω_m to obtain a record of the motion. To excite a desired mechanical mode, the amplitude of an auxiliary laser is modulated at Ω_m. When the modulation is turned off, the oscillation amplitude decays according to $x(t) = x(0)\exp[-\Omega_m t/(2Q)]$, as shown in Extended Data Fig. 2a. From a fit we extract a quality factor of $Q = 1.03 \times 10^9$.

When measuring such extreme quality factors, it is important to ensure that the decay is not modified by any residual dynamical effects due to photothermal or radiation-pressure backaction. In Extended Data Fig. 2b, we confirm that the measured Q does not depend on laser power, as would be expected for these effects. We also conduct a 'stroboscopic' ringdown measurement, in which the motion was probed for only brief moments (duty cycle of about 4%, period of about 0.5 min). The continuous and stroboscopic ringdowns overlap well, yielding Q values of 1.03×10^9 and 1.02×10^9, respectively. The inset of Extended Data Fig. 2a shows the power spectral density of the continuous ringdown data. The width of this peak is Fourier-limited to 1.1 mHz for these data and thereby confirms the absence of substantial dephasing: the energy decay rate was found (by ringdown) to be 1.1 mHz.

Experimental set-up. Extended Data Fig. 3 shows more details about the set-up for the experiments described in the main text. A Ti:sapphire laser (red) at $\lambda \approx 795$ nm is used to probe the frequency fluctuations of an optical cavity mode whose linewidth is $\kappa/(2\pi) = 15.9$ MHz. To stabilize the laser frequency relative to the optomechanical cavity, we implement a Pound–Drever–Hall scheme[49], using a phase modulator on the probe beam. This phase modulator is also driven with a coherent tone at ν_{cal}, to calibrate the transduction of optical frequency fluctuations into detected voltage fluctuations[32]. At the wavelength of this probe beam, the reflectivities of the two cavity mirrors differ greatly, forming a strongly asymmetric optical resonator. To detect as much of the cavity light as possible, we drive the cavity through the higher-reflectivity port while detecting the light leaving the more transmissive port. We perform a phase-sensitive measurement on the transmitted light by means of a balanced homodyne receiver.

To stably measure the optical phase of the signal beam, on which the mechanical displacement information is imprinted, we stabilize the path difference of the signal and local oscillator arms. A feedback loop actuates a piezo-controlled mirror in the local oscillator path, minimizing the d.c. component of the photocurrent[50]. The information about the mechanics is contained in the a.c. part of the photocurrent, which is digitally acquired both from a data acquisition card to perform a Fourier analysis and from a digital lock-in amplifier to analyse the time evolution (Supplementary Information).

An auxiliary Ti:sapphire laser (blue) at $\lambda_{aux} \approx 796$ nm is frequently used in the experiment. To avoid unwanted interference, its polarization is orthogonal to the probe laser and it is locked to a different longitudinal cavity mode, whose linewidth is $\kappa_{aux}/(2\pi) = 12.9$ MHz. In the experiment described in Fig. 2, this laser provides the sideband cooling and acts as a source of strong quantum backaction. In the feedback cooling experiment (Fig. 4), the auxiliary laser is used (in combination with an amplitude modulator) to exert a force on the mechanical resonator via radiation pressure, that is, to actuate the feedback force. For this feedback, a field-programmable gate array (FPGA)-based digital controller (RedPitaya 125-14; https://redpitaya.com) is used to bandpass-filter the a.c. homodyne photocurrent close to the mechanical mode to be cooled. The filter is implemented in an open-source, Python-based software module[51] (https://github.com/lneuhaus/pyrpl), whereby the built-in I/Q modulation capability enables filters with continuously tunable phase. The processed signal is amplified and sent to a fibre-integrated optical amplitude modulator on the auxiliary beam. In the actual experiment we use several FPGA controllers. One of them is devoted to cooling the defect mode of interest, using the transfer function $h_{main}(\Omega)$ given in equation (2). An electronic switch is inserted just after this controller to toggle the feedback force on and off to

measure transient dynamics (Supplementary Information). All other controllers can be grouped in a single transfer function $h_{aux}(\Omega)$, which is used to cool some of the low-frequency modes that correspond to motion of the entire Si$_3$N$_4$ membrane structure, as well as defect modes C and D. This is needed to avoid large frequency fluctuations and keep the whole system stable. This auxiliary controller is always on in the experiments reported in Figs. 3 and 4.

Optomechanical assembly. We largely use the same optomechanical assembly and optical characterization techniques as described previously[28], combining them here with a soft-clamped membrane[26]. In this membrane-in-the-middle geometry[27], the main optomechanical parameters—the optical-mode resonance frequency, the vacuum optomechanical coupling g_0, the cavity linewidth κ and the cavity outcoupling η_c—depend on the position z_m of the centre of mass of the membrane relative to the intracavity standing wave. Because the position of the membrane is constrained by the cavity assembly, we use a laser whose wavelength can be tuned (over about 200 nm) to control these parameters. Tuning the laser to the next longitudinal optical resonance introduces one more antinode in the intracavity standing wave, effectively changing the position of the membrane relative to the standing wave.

To predict how the other parameters behave as a function of λ, we use a transfer matrix model[52]. In this approach, the optomechanical system is modelled as a stack of component transfer matrices, whose total behaviour can be analysed to predict system parameters. We measure the shift of the optical resonance frequencies for several longitudinal modes and fit them with the transfer matrix model to estimate a cavity length $L = 1.6$ mm and a membrane position $z_m = 0.5$ mm relative to the flat, transmissive mirror. By using an independent measurement of the transmissivity of the mirrors, we also predict the cavity outcoupling $\eta_c = \kappa_{out}/\kappa$ to be modulated between 0.88 and 0.95, depending on membrane position. With the known laser wavelength and inferred z_m, the transfer matrix model predicts a unique value for η_c. We use this to obtain an estimate of g_0 from an OMIT trace (η_c links the measured output power with the intracavity photon number) and find excellent agreement with the g_0 obtained from the quantum backaction calibration, which is independent of η_c (Supplementary Information). No other results reported here depend on η_c.

To measure the cavity linewidth κ, we sweep a phase-modulated laser across the cavity resonance and measure the transmitted intensity. The central feature is fitted with a Lorentzian and its linewidth is converted to frequency units using the phase-modulation sidebands as frequency markers. During the sweep the auxiliary laser is locked to the red side of a different cavity mode to laser-cool the mechanical modes of the entire membrane structure; large-amplitude excursions of these modes can otherwise lead to artificial broadening of the cavity line shape.

Detection efficiency budget. High detection efficiency is critical for our quantum measurements. To increase the quantum efficiency of the photodiodes, we removed the protective glass window. From the measured responsivity, we estimate a quantum efficiency of 93%, which is 2% below the specified values. We believe this difference comes from minor damage during the window removal process. In Extended Data Table 1 we report a breakdown of contributions to the total detection efficiency. Adding up all losses gives an expected efficiency of $\eta_{det} = 80\%$. However, we measure directly the losses between just after the cryostat window and just before the photodetection to be 92% instead of the expected 95%, which reduces the detection efficiency to $\eta_{det} = 77\%$. Electronic noise in all measurements is around 1% of the optical vacuum noise level.

Calibration of g_0 via quantum noise thermometry or OMIT. We implement two independent methods to measure the single-photon optomechanical coupling g_0 between a given cavity mode and the mechanical mode.

First, we lock the probe laser on the red side of the cavity and modulate its phase with a coherent tone. We observe OMIT[30] in the optical response function when the frequency of that tone is swept and the intensity of the transmitted beam is detected directly. If the laser detuning Δ and the cavity linewidth κ are measured independently then the measured trace can be fitted to extract the light-enhanced coupling g. From it, the single-photon coupling g_0 can be derived if the optical losses to the detector and the cavity outcoupling η_c are known.

In Extended Data Fig. 4 we show a series of OMIT traces with different detunings, with the corresponding fits. While the optical losses in the detection path are measured to be 5%, the cavity outcoupling cannot be measured directly. Therefore, we assume the outcoupling from the transfer matrix model for this particular cavity mode, $\eta_c = 95\%$. With this assumption, we estimate a single-photon coupling of $g_0/(2\pi) = 129^{+2}_{-3}$ Hz.

The second method to measure g_0 relies on precise knowledge of the temperature of the mechanical mode. When that is the case, we can compare the measured mechanical energy to a known frequency modulation to obtain g_0. This method is explained in more detail in Supplementary Information, but the result is $g_0/(2\pi) = 127 \pm 2$ Hz. The agreement between the two methods is particularly meaningful because they make very different assumptions. In brief, the first is essentially a calibration based on intracavity photon occupation, while the second is based on a certain mechanical phonon occupation.

Data availability

Source Data for Figs. 1–5 are provided with the online version of the paper and are available in the UCPH ERDA repository (https://doi.org/10.17894/ucph.2612dd59-20ab-40d2-a33d-f53e4428c4cd).

49. Black, E. D. An introduction to Pound-Drever-Hall laser frequency stabilization. *Am. J. Phys.* **69**, 79–87 (2001).

50. Leonhardt, U. *Measuring the Quantum State of Light* Ch. 4.2 (Cambridge Univ. Press, Cambridge, 1997).

51. Neuhaus, L. et al. PyRPL (Python Red Pitaya Lockbox) — an open-source software package for FPGA-controlled quantum optics experiments. In *2017 Conference on Lasers and Electro-Optics Europe and European Quantum Electronics Conference* https://doi.org/10.1109/CLEOE-EQEC.2017.8087380 (Optical Society of America, 2017).

52. Jayich, A. M. et al. Dispersive optomechanics: a membrane inside a cavity. *New J. Phys.* **10**, 095008 (2008).
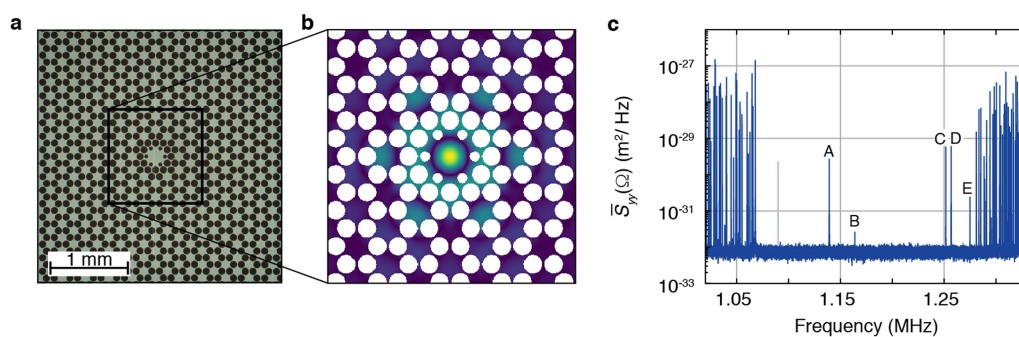
Extended Data Fig. 1 | Soft-clamped membrane. a, Photograph of the soft-clamped membrane. **b**, Simulated displacement pattern of defect-localized mode A. **c**, Mechanical spectrum of the lowest-frequency bandgap, with defect-localized modes labelled from A to E. The grey peak at 1.09 MHz is a phase-calibration tone.
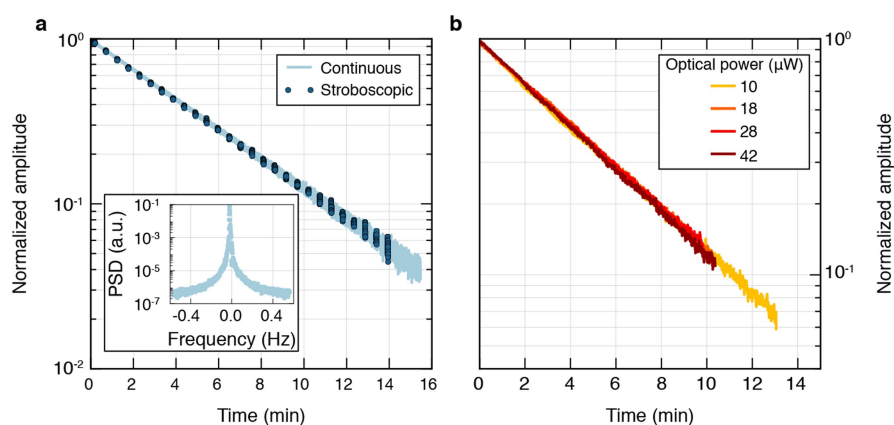
Extended Data Fig. 2 | Mode A ringdowns. a, Ringdowns with continuous and stroboscopic optical monitoring. The inset shows the power spectral density (PSD) of the continuous ringdown data.

b, Ringdowns at different continuous optical powers. The Q values extracted are 1.02×10^9, 1.06×10^9, 1.07×10^9 and 1.04×10^9 from high to low optical power.
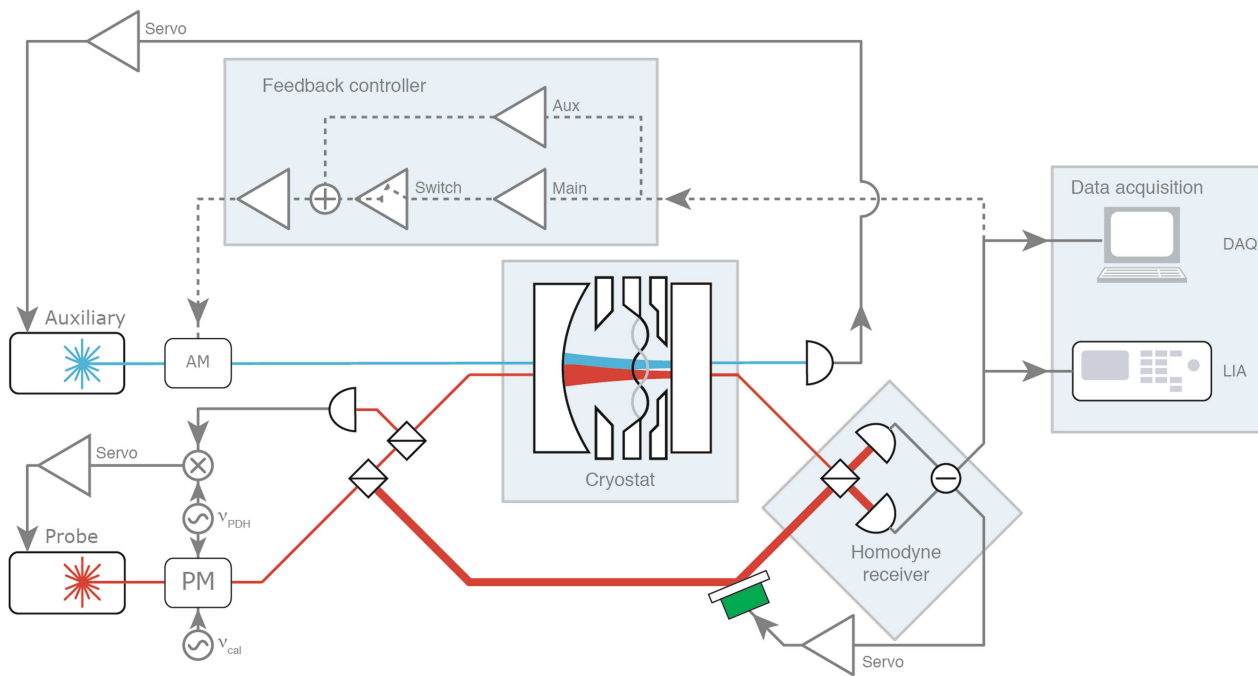
Extended Data Fig. 3 | Experimental set-up. An overview of the optical and electronic scheme used in the experiments is shown. AM, amplitude modulator; PM, phase modulator; DAQ, data acquisition card; LIA, lock-in amplifier; aux, auxiliary; ν_{PDH}, Pound–Drever–Hall modulation frequency; ν_{cal}, calibration tone frequency.
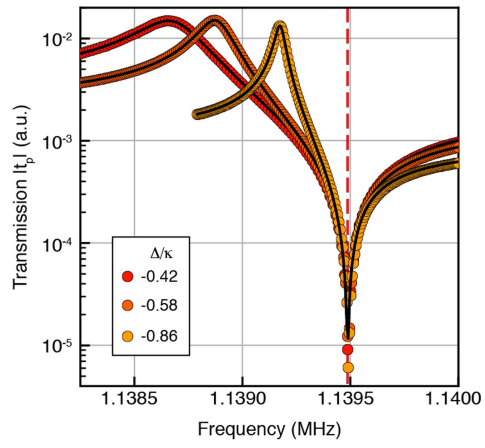
Extended Data Fig. 4 | OMIT. Measured traces of the transmission $|t_p|$ are shown for different laser detunings, close to the mechanical frequency Ω_m (dashed red line). Black lines are theoretical fits.

Extended Data Table 1 | Contribution to detection efficiency

Optical element	Value	Origin
Cavity outcoupling	95%	TMM
Cavity window	99.6%	Specs
Lens	99.6%	Specs
PBS, transmission	99%	Measured
Lens	99.6%	Specs
Waveplate	99.2%	Specs
PBS, transmission	99%	Measured
PBS, reflection	99.5%	Specs
Diode quantum efficiency	93%	Measured
Interference visibility	98%	Measured

PBS, polarizing beam splitter; TMM, transfer matrix model.